# Solving Non-linear Elasticity BVPs in FEniCS

## Bifurcations and Buckling of Beams


Christiana Mavroyiakoumou

University of Oxford

A special topic report submitted for the degree of

*M.Sc. in Mathematical Modelling and Scientific Computing*

Trinity 2017

# Contents



**Acknowledgements.** Special thanks to Professor Patrick Farrell for teaching me the courses: C6.4 Finite Element Method for PDEs and Python in Scientific Computing and introducing me to FEniCS, a very powerful tool for solving partial differential equations.

# 1 Introduction and Motivation

In this report, we are concerned with nonlinear elasticity problems in different dimensions. One of the problems we discuss are nonlinear equations of the form

$$F(u, \lambda) = 0, \tag{1.1}$$

as presented in [KA68]. Here, $F$ represents a nonlinear operator which depends on the parameter $\lambda$ operating on the unknown function $u$. There are two main questions to ask. The first question to ask is whether or not (1.1) has any solution $u$ for a given value of $\lambda$. If a solution does exist, then we would like to know how many solutions arise and then how this number varies with $\lambda$.

The process of bifurcation whereby a given solution of (1.1) splits into two or more solutions as $\lambda$ passes through a critical value $\lambda_c$, called the bifurcation point, is particularly interesting. We consider a basic example of a bifurcation phenomenon, that of the deformation of a slender beam under a load which was first analysed by Euler and Bernoulli [Rei69].

It can be observed that as the load $\lambda$ increases gradually from zero, the beam first deforms by thickening and shortening but with its centreline still remaining straight. However, after a critical value $\lambda_c$ the beam bends out of plane, resulting in a large deformation known as *buckling*. This phenomenon is illustrated in Figure 1.1.

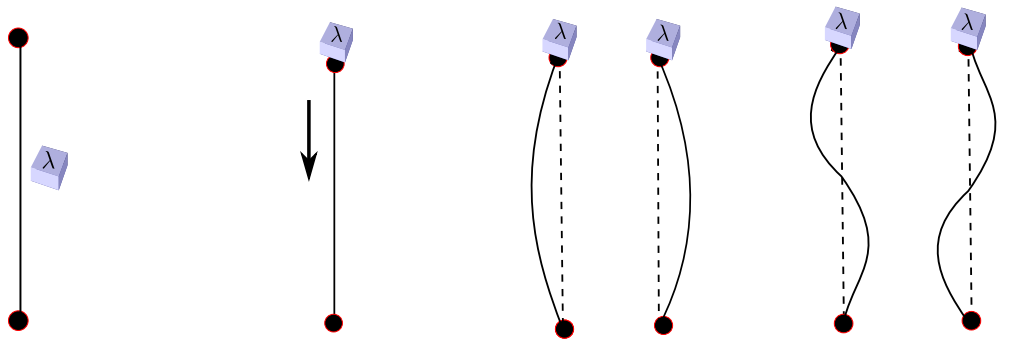


(a) Undeformed. (b) $\lambda = \lambda_c$. (c) $\lambda > \lambda_c$ (1st). (d) $\lambda > \lambda_c$ (2nd).

Figure 1.1: Schematic diagrams of the deformation of a vertical beam when a load $\lambda$ is placed at its top. There is a qualitative change in the deformation of the beam around a critical value $\lambda_c$ of the load.

Even though the classical linear theory of elasticity predicts that there is a unique solution to any problem, this is insufficient to describe buckling and so we need to

employ a nonlinear theory. To visualise bifurcations we construct a so-called bifurcation diagram, where the $y$-axis is a functional $J(u)$, and the $x$-axis is the parameter $\lambda$. Using a bifurcation diagram, we can see the structure of the solution curves in the parameter space. Note that their intersection point is known as the bifurcation point. A schematic of a bifurcation diagram is depicted in Figure 1.2.

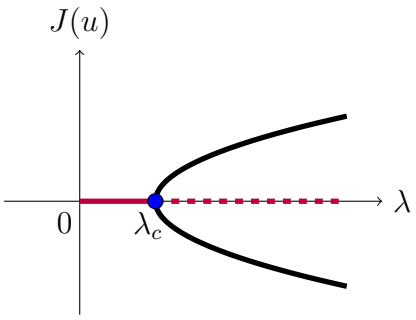


Figure 1.2: Schematic of a bifurcation diagram. The blue circle represents the bifurcation point and it is at the critical load parameter $\lambda_c$. In this pitchfork bifurcation diagram, the stable solutions are drawn with a solid line and the unstable ones with a dashed line.

Due to the nonlinear nature of the problem, constructing a bifurcation diagram and analysing the behaviour of the solution of (1.1) can be complex. However, it is still possible to investigate these systems using iterative methods. Such methods try to find a better approximation to the solution of (1.1), if we provide an initial guess for the solution.

Newton's method is one of the most widely used iterative methods. This is because it has fast convergence properties close to the actual roots of the equation. However, if we started instead far away from a solution, then Newton's method could result in fast divergence. This is evident especially in the case of highly nonlinear problems.

Iterative methods enable us to compute bifurcation diagrams using *numerical continuation*. If an initial point is given on the solution branch, then we can use this point as the initial guess to compute a solution on the same solution branch but for a different value of the parameter. This means that the use of iterative methods allows us to continue our solution along a solution branch. Furthermore, note that if the steps taken are small enough such that the iterative methods are ensured to converge at each step, then full solution branches can be traced out by proceeding in an iterative manner along solution branches.

## 1.1 Finite Elements in Elasticity with FEniCS

Finite elements are one of the most widely used methods for finding the deformations of elastic materials subjected to loads. Here, we present one-dimensional beam models (with various boundary conditions) but also two- and three-dimensional hyperelastic models. Due to the nonlinearity of the governing equations, a finite element approach implemented in FEniCS is used to find numerical solutions to the model equations.

Very briefly, the finite element method goes as follows: Given a function (Hilbert) space $V$, a continuous and coercive bilinear form $a(u, v)$, and a continuous linear form $L(v)$, we can now consider the variational formulation which is to find

$$u \in V \text{ such that } a(u, v) = L(v) \quad \text{for all } v \in V. \tag{1.2}$$

This has a unique solution by the Lax-Milgram theorem [All07, Th. 3.3.1]. The *internal approximation* of (1.2) consists of replacing the function space $V$ by a finite dimensional subspace $V_h$, or in other words, consists of finding

$$u_h \in V_h \text{ such that } a(u_h, v_h) = L(v_h) \quad \text{for all } v_h \in V_h. \tag{1.3}$$

Solving a physical problem with FEniCS consists of the following steps:

1. Identify the PDE and its boundary conditions.
2. Reformulate the PDE problem as a variational problem.
3. Write code in Python using Unified Form Language developed under FEniCS. This includes the formulas in the weak form and definitions of input data.
4. Add statements in the program for solving the variational problem, computing derived quantities such as $\nabla u$, and finally visualising the results in ParaView.

# 2 Deflection of a Diving Board

Let us consider a horizontal beam and describe its deformation using arclength $s$ along the centreline and angle $\theta(s)$ between the centreline and the $x$-axis as in [HKO09, Sec. 4.9.2]. Note that $s$ can be viewed as a Lagrangian coordinate, fixed in the deforming beam. The displacement is given in parametric form as $x = x(s)$ and $w = w(s)$, where we have

$$\frac{\mathrm{d}x}{\mathrm{d}s} = \cos\theta \qquad \text{and} \qquad \frac{\mathrm{d}w}{\mathrm{d}s} = \sin\theta. \tag{2.1}$$

In Figure 2.1 we show the bending moment $M$ and also the sign convention for the tangential and normal forces ($T$ and $N$) at the ends of a beam.

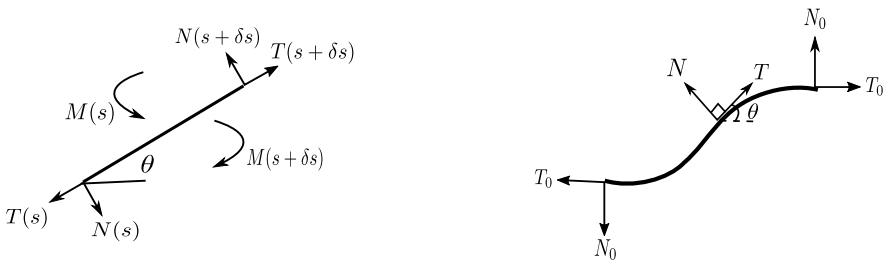


Figure 2.1: Forces and moments and sign convention at the ends of the beam.

Ignoring inertia and body forces (e.g. ignoring $\rho\delta s$) and balancing forces horizontally and vertically on a small segment of the beam, we get respectively

$$(\rightarrow) \quad [T(s+\delta s) - T(s)]\cos\theta + [N(s) - N(s+\delta s)]\sin\theta = 0, \tag{2.2}$$

$$(\uparrow) \quad [N(s+\delta s) - N(s)]\cos\theta + [T(s+\delta s) - T(s)]\sin\theta = 0. \tag{2.3}$$

Now, dividing (2.2) and (2.3) by $\delta s$ and taking the limit $\delta s \to 0$ yields

$$\frac{\mathrm{d}}{\mathrm{d}s}(T\cos\theta - N\sin\theta) = 0, \qquad \frac{\mathrm{d}}{\mathrm{d}s}(N\cos\theta + T\sin\theta) = 0. \tag{2.4}$$

In equilibrium, the moments also balance and, following the convention that a positive shear force creates a positive moment, we have

$$\frac{\mathrm{d}M}{\mathrm{d}s} - N = 0. \tag{2.5}$$

If we apply a force $(T_0, N_0)$ at the right-hand end, and an equal and opposite force at the left-hand end as in Figure 2.1, then it follows that

$$T = T_0\cos\theta + N_0\sin\theta, \qquad N = N_0\cos\theta - T_0\sin\theta. \tag{2.6}$$

Assuming that the elastica is sufficiently thin, we can use as a constitutive relation, relating the bending moment $M$ to the curvature $\frac{\mathrm{d}\theta}{\mathrm{d}s}$, the following equation

$$M = -EI\frac{\mathrm{d}\theta}{\mathrm{d}s}. \tag{2.7}$$

Combining (2.5) with (2.6) and (2.7) yields the *Euler-Bernoulli* equation

$$EI\frac{\mathrm{d}^2\theta}{\mathrm{d}s^2} + N_0\cos\theta - T_0\sin\theta = 0. \tag{2.8}$$

Let us first consider the steady deformation of a diving board of length $L$ where we neglect gravitational forces. Suppose that the diving board is clamped horizontally at $s = 0$ ($\theta(0) = 0$) and a downward force $F$ is applied to the other end which is free to move (zero moment). We thus have $T_0 = 0$ and we can rewrite $N_0$ as $N_0 = -F$. So (2.8) becomes

$$EI\frac{\mathrm{d}^2\theta}{\mathrm{d}s^2} = F\cos\theta, \qquad \theta(0) = \frac{\mathrm{d}\theta}{\mathrm{d}s}(L) = 0. \tag{2.9}$$

To solve this problem in FEniCS we need to turn (2.9) into variational form.

## 2.1 Variational Statement of the Problem

We non-dimensionalise the problem by scaling $s = L\hat{s}$ and dividing (2.9) by $EI$ to obtain the normalised problem (dropping hats)

$$\frac{\mathrm{d}^2\theta}{\mathrm{d}s^2} - \delta\cos\theta = 0, \qquad \theta(0) = \frac{\mathrm{d}\theta}{\mathrm{d}s}(1) = 0, \tag{2.10}$$

where we have a single dimensionless parameter $\delta = \frac{FL^2}{EI}$. Note that this dimensionless parameter $\delta$ measures the applied force $F$ relative to the stiffness of the board. The force $F$, the Young's modulus, $E$, as well as the second moment of inertia, $I$, are problem dependent. For the remainder of this problem, we choose the following parameters for the diving board: $E = 1.2 \times 10^9$ Pa, $L = 1$ m and a rectangular cross section of width $b = 40$ cm and height $d = 5$ cm, with moment of inertia $I = \frac{1}{12}bd^3$. These are estimates for what a real diving board would be.

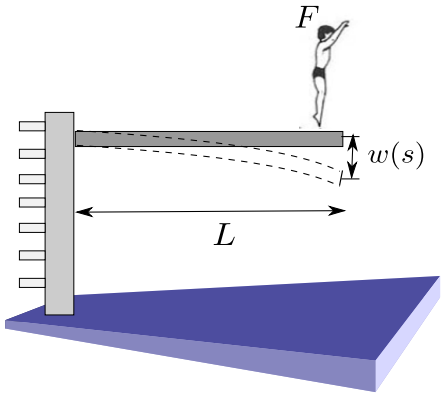


We solve (2.10) by employing the finite element method (FEM). In order to use this method we need to cast the problem into variational form. The main idea is to multiply (2.9) by a function $v$, integrate the resulting equation over $\Omega$ which in this case is just $x \in [0, 1]$, and perform integration by parts of terms with second-order derivatives. The function $v$ which multiplies (2.9) is called a *test function* and the unknown function $\theta$ that we wish to approximate is the *trial function*. Suitable function spaces must be specified for the test and trial functions.

Let $v$ be any sufficiently regular function such that $v(0) = 0$. We define the space

$$V = \{v \in H^1(0, 1) : v(0) = 0\}. \tag{2.11}$$

This definition makes sense because we know $H^1(\Omega)$ functions in one dimension are continuous and and we can thus evaluate $v$ at the left endpoint. If we multiply both sides of (2.10) by $v \in V$ and integrate, we obtain

$$\int_0^1 \left(\frac{\mathrm{d}^2\theta}{\mathrm{d}s^2} - \delta\cos\theta\right) v \,\mathrm{d}s = 0. \tag{2.12}$$

We wish to reduce the regularity requirements on $\theta$ by shifting one of the derivatives from $\theta$ onto $v$; this is achieved by *integration by parts*. As we choose $v$ to vanish on $x = 0$, and using the boundary condition $\frac{\mathrm{d}\theta}{\mathrm{d}s}(1) = 0$, this reduces to

$$\int_0^1 \left( \frac{\mathrm{d}\theta}{\mathrm{d}s} \frac{\mathrm{d}v}{\mathrm{d}s} + \delta v \cos\theta \right) \mathrm{d}s = 0. \tag{2.13}$$

Putting this into FEniCS we can obtain the deflection of the diving board under some downward force. For a more realistic visualisation of the process that takes place when we clamp one end of the board and apply a downwards force pointwise at the free end, we plot the deflection of the diving board in $(x(s), w(s))$ as shown in Figure 2.2. We show the diving board profile corresponding to different applied forces, and it is clear how the force causes the deflection to increase. See Appendix A for more details on the diving board example.

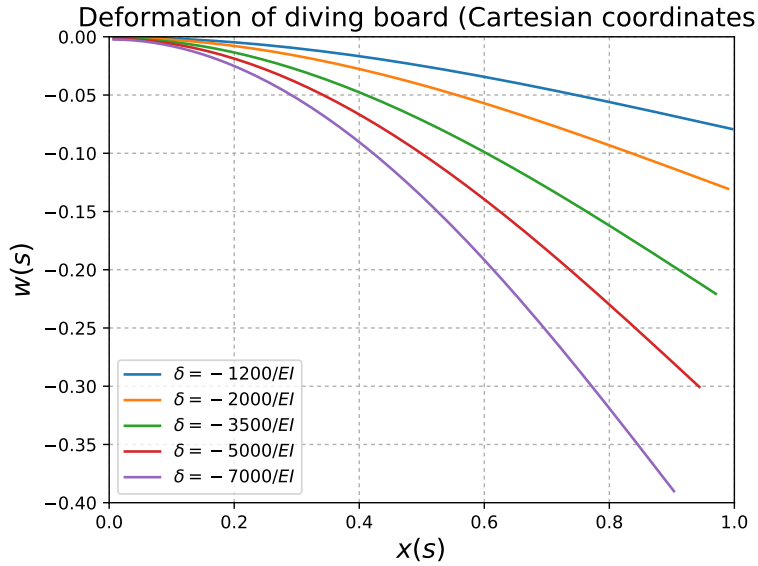


Figure 2.2: Diving board centreline $(x(s), w(s))$ for different values of the dimensionless force parameter $\delta$.

## 2.2 Computing Convergence Rates

The method of manufactured solutions (MMS) is a general procedure that can be used to construct analytical solutions to the differential equations that form the basis of our simulation code [Roa02]. Note that even though the resulting solutions might not be of any physical relevance, they can be used as benchmark solutions for verification tests. The accuracy of the code is determined by running test problems

on systematically refined grids and then comparing the output with the manufactured analytical solution. We then compare the error against the theoretical order of accuracy inherent in the discretisations of the code.

Suppose that the differential equation we wish to solve has the form

$$\mathrm{D}(u) = 0, \tag{2.14}$$

where $u$ is the unknown variable and $\mathrm{D}(\cdot)$ is a differential operator whose form depends on the governing PDE. In MMS, we choose a $u^\star$ that satisfies the appropriate boundary conditions. Since $u^\star$ does not necessarily satisfy the original governing equation (2.14), a corresponding source term $f$ is manufactured by applying the differential operator to $u^\star$ in order to balance

$$\mathrm{D}(u^\star) = f. \tag{2.15}$$

Therefore, we can test our numerical code — initially designed to solve (2.14) — by finding a numerical solution $u_{\text{approx}}$ to the new equation $\mathrm{D}(u) = f$ for which we have an exact analytical solution given by the manufactured $u^\star$. The error is $e = u^\star - u_{\text{approx}}$.

For problem (2.10), we manufacture a solution $\theta_{\text{exact}}$ that is not symmetric, it is not a polynomial, and that satisfies $\theta(0) = \frac{\mathrm{d}\theta}{\mathrm{d}s}(1) = 0$, e.g.

$$\theta_{\text{exact}} = 1 - \cos\left[\frac{2\pi s}{1 + s(1-s)}\right]. \tag{2.16}$$

In Table 1, we show the computed relative residual norms after each iteration of the Newton solver for the nonlinear model problem using $\mathcal{P}_1$ and $\mathcal{P}_2$ elements. We denote by $\mathcal{P}_k$ the set of polynomials which have real coefficients and one real variable, and degree less than or equal to $k$. Quadratic convergence is observed when using $\delta = -\frac{5000}{EI}$, for both $\mathcal{P}_1$ and $\mathcal{P}_2$ elements.

| Iteration | Relative Residual Norm $\mathcal{P}_1$ | Relative Residual Norm $\mathcal{P}_2$ |
|---|---|---|
| 1 | 1.085e-02 | 1.085e-02 |
| 2 | 1.530e-06 | 1.530e-06 |
| 3 | 2.416e-12 | 2.759e-11 |

Table 1: Relative residual norms computed when solving (2.10).

The results are shown in Figures 2.3 and 2.4. The source function $f$ to be used in the new equation is found using MAPLE. For the code, see Appendix B. Let us remark that using a logarithmic scale enables us to visualise convergence rates as the slope of the logarithm of the error as a function of the logarithm of the resolution $h$.

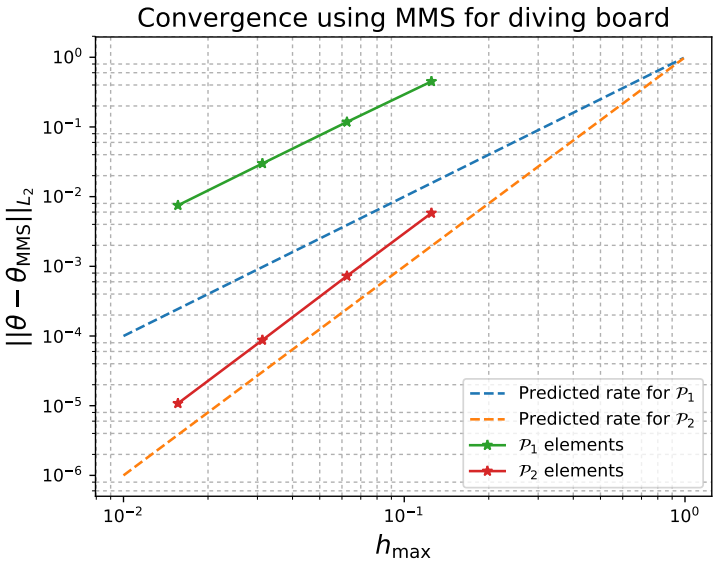


Figure 2.3: We test the convergence of the numerical solution $\theta$ to the test solution (2.16) in the $L_2$-norm for first and second order Lagrange elements as a function of the mesh size $h_{\max}$, using MMS. The dotted lines show the theoretical convergence rates, $\mathcal{O}(h^2)$ for $\mathcal{P}_1$-elements and $\mathcal{O}(h^3)$ for $\mathcal{P}_2$-elements, as predicted in [All07, pp. 167]. Note that predicted lines are just a reference for gradient.

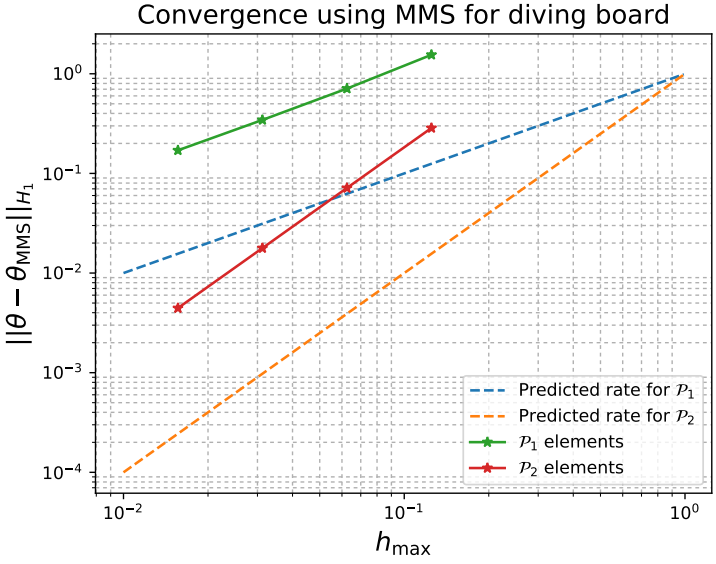


Figure 2.4: We test the convergence of the numerical solution $\theta$ to the test solution (2.16) in the $H_1$-norm for first and second order Lagrange elements as a function of the mesh size $h_{\max}$. The dotted lines show the theoretical convergence rates, $\mathcal{O}(h)$ for $\mathcal{P}_1$-elements and $\mathcal{O}(h^2)$ for $\mathcal{P}_2$-elements, as predicted in [All07, pp. 167].

# 3 Deformation of a Slender Vertical Beam

Consider the deformation of a slender vertical beam under compression by a load [HKO09]. Let us focus on a model problem of a beam with length $L = 1$ which is clamped at both ends, is subject to a compressive force $P = -T_0$ and has zero transverse force.

This is governed by Euler's elastica equation

$$\frac{\mathrm{d}^2\theta}{\mathrm{d}s^2} + \frac{P}{EI}\sin\theta = 0, \tag{3.1}$$

with boundary conditions $\theta(0) = \theta(1) = 0$, where $s$ is the arclength along the beam and $\theta(s)$ is the angle relative to the vertical axis. This is a nonlinear eigenvalue problem. Notice that $\theta \equiv 0$ is always a solution, and we are seeking values of the applied force $P$ for which (3.1) admits nonzero solutions. If such solutions exist then they correspond to buckling of the beam. Note that (3.1) can also be written as

$$\frac{\mathrm{d}^2\theta}{\mathrm{d}s^2} + \lambda^2\sin\theta = 0, \qquad \theta(0) = \theta(1) = 0, \tag{3.2}$$

where $\lambda^2 = \frac{P}{EI}$. This system is a basic model problem for bifurcation analysis [MH94, Ch. 7]. One central task of bifurcation theory is to determine the effect of varying the parameter on the number of solutions to an equation. The problem was largely solved by Euler and the relevant bifurcation diagram is similar to that shown in Figure 3.2.

As we will discuss now, the bifurcation points $\lambda = k\pi$, with $k \in \mathbb{N}_+$ can be readily computed. They are the eigenvalues of the linearised problem about the trivial solution $\theta = 0$, i.e. small deflections, that is $\theta = 0 + \varphi + \mathcal{O}(\varphi^2)$ for $\varphi \ll 1$

$$\frac{\mathrm{d}^2\varphi}{\mathrm{d}s^2} + \lambda^2\varphi = 0, \qquad \varphi(0) = \varphi(1) = 0. \tag{3.3}$$

Therefore, if $\theta$ is small, then (3.1) reduces to the linear eigenvalue problem (3.3), for which the solution to the second order differential equation (3.3) is

$$\varphi = \begin{cases} A\sin(k\pi s) & \text{for } \lambda = k\pi,\ k \in \mathbb{N}_+, \\ 0 & \text{otherwise.} \end{cases} \tag{3.4}$$

Thus, $\varphi = 0$ unless $\lambda$ (or equivalently, $P$) takes one of a discrete set of critical values. This corresponds to the vertical slender beam remaining straight. When $\lambda = k\pi$, with $k \in \mathbb{N}_+$, $\varphi = A\sin(k\pi s)$, which corresponds to the beam buckling with shape $\sin(k\pi s)$. See the expected buckling shapes for $k = 1, 2, 3$ in Figure 3.1.

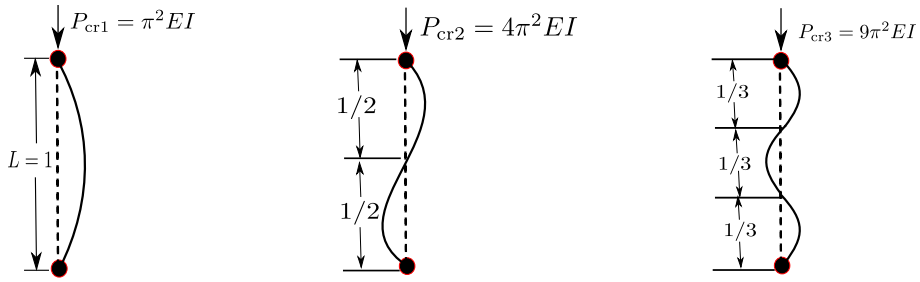


(a) Mode shape 1 ($k = 1$) (b) Mode shape 2 ($k = 2$) (c) Mode shape 3 ($k = 3$)

Figure 3.1: First three buckling mode shapes for the Euler vertical buckling beam.

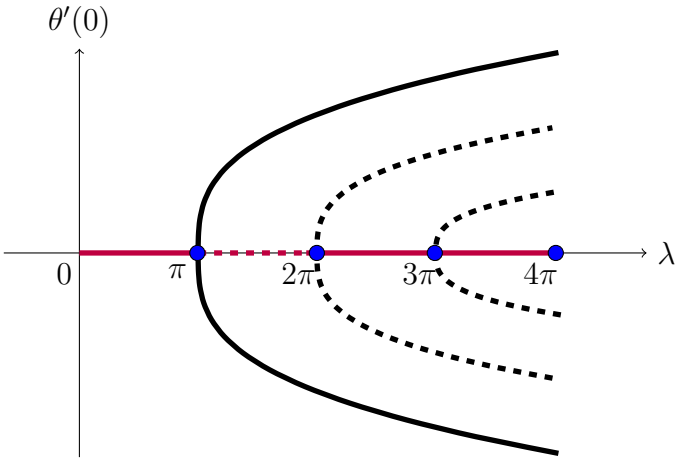


Figure 3.2: Schematic of the bifurcation diagram for the Euler 1D elastica equation (3.2) as a function of $\lambda$. This is similar to [MH94, Fig. 7.1.3]. The blue circles represent the bifurcation points, the stable solutions are drawn with a solid line and the unstable ones with a dashed line. Also for $\lambda < \pi$, no buckling is possible and the solution curves do not intersect as shown in [KA68, pp. 12].

The $\lambda$-axis is called the *trivial branch of solution pairs* and the other *nontrivial* branches, correspond to the buckled states. One can observe that there are at least three solution pairs when $\pi < \lambda < 2\pi$, at least five solution pairs when $2\pi < \lambda < 3\pi$, etc. For the simple one-dimensional elastica model, there are countably infinite such $\lambda$'s which correspond to the eigenvalues of (3.3).

We shall now dissect the FEniCS program written to solve (3.2) in detail. The program is written in the PYTHON programming language. The listed FEniCS program defines a finite element mesh, the discrete function space $V$ corresponding to this mesh and the element type. It also defines the boundary conditions for $\theta$ (which is $u$ in our code) and the variational formulation of the problem. Then, the unknown function $u$ is computed and we can investigate $u$ visually using PARAVIEW [LMW12].

Since we are concerned with a one-dimensional problem with $x \in [0, 1]$, we need to define a uniform finite element mesh as

```
mesh = UnitIntervalMesh(32)
```

where the mesh consists of cells which are triangles with straight sides. The parameter 32 tells us that the unit interval is divided into 32 intervals, with 33 total vertices.

We can now define a discrete function space $V$ over the constructed mesh

```
V = FunctionSpace(mesh, "Lagrange", 1)
```

This means that we discretise (3.2) using piecewise linear Lagrange elements. This is a triangle with nodes at the three vertices. Note that for (3.2) we define the function space as $V = H_0^1 = \{v \in H^1(\Omega) : v|_\Gamma = 0\}$ which is equivalent to $v(0) = 0 = v(1)$.

We next define the test and trial functions as follows

```
u = Function(V)
v = TestFunction(V)
```

We have Dirichlet boundary conditions given by $\theta(0) = \theta(1) = 0$ and these are translated in FEniCS as

```
bc = DirichletBC(V, 0.0, "on_boundary")
```

Now that we have all the components needed to specify the problem, we can write the variational form of (3.2)

```
F = inner(grad(u), grad(v))*dx - lambd**2*sin(u)*v*dx
```

where we choose $\lambda$ to be a particular constant. Note that we later use continuation which is a very powerful algorithm for solving difficult nonlinear problems. The idea is that we construct an initial guess by solving an easier problem.

We also set a good initial guess to ensure faster convergence

```
u.interpolate(Expression("-sin(x[0])",degree=2))
```

We solve (3.2), which we discretised using FEniCS and PETSc, from $\lambda = 0$ to $\lambda = 4\pi$ with numerical continuation. We choose to terminate Newton's method with failure if convergence does not occur within the first 100 iterations.

To apply continuation in FEniCS, we update the parameter in a loop and solve

```
# solve the variational problem using numerical continuation
for lambd_val in list(np.linspace(3*pi-0.01, 4*pi, 200)):
    lambd.assign(lambd_val)
    solve(F==0, u, bc, solver_parameters={"newton_solver":
    {"maximum_iterations": 100}})
```

Listing 3.1: Part of Python code for Euler's 1D elastica problem (3.2).

A number of solutions resulting from choosing different values for $\lambda = k\pi$ for $k \in \mathbb{N}_+$ are presented in Figure 3.3. We can see different buckled modes emanating from the trivial branch.

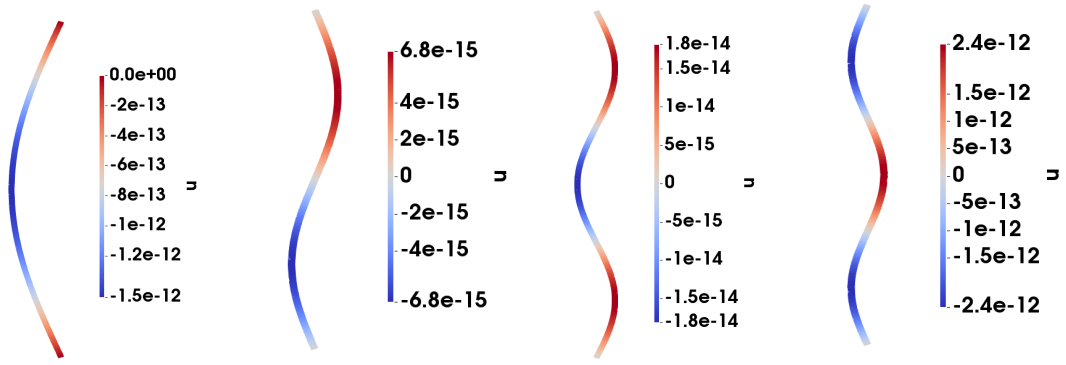


(a) First. (b) Second. (c) Third. (d) Also third.

Figure 3.3: We observe three eigenmodes that arise under different loads. All subfigures are plotted with different color bars. Also notice that (c) and (d) have opposite signs corresponding to solutions in the upper and lower branches of Figure 3.2. There is also a difference in amplitude because although they lie on solution branches of the third eigenmode with opposite sign, they have different $\lambda$ forcing. All of these have the expected sinusoidal shape.

## 3.1 Computing Convergence Rates

The problem of the deformation of a vertical slender beam clamped at both ends is very similar to that of the deformation of a diving board presented in Section 2. Therefore, we expect that the convergence rates for both of these problems are similar. Indeed, using the method of manufactured solutions, we construct the same $\theta_{\text{exact}}$ given by

$$\theta_{\text{exact}} = 1 - \cos\left[\frac{2\pi s}{1 + s(1-s)}\right], \tag{3.5}$$

since it satisfies both boundary conditions $\theta(0) = \theta(1) = 0$.

The convergence plots for the case of the deforming Euler's elastica problem are presented in Figure 3.4.

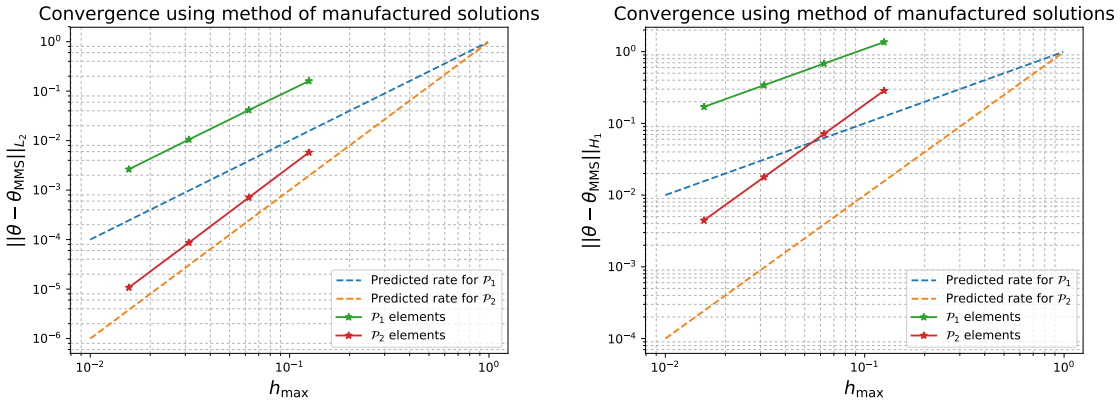


(a) Convergence in the $L_2$-norm.

(b) Convergence in the $H_1$-norm.

Figure 3.4: Convergence plots for the clamped-clamped elastica problem (3.2).

# 4 Hyperelasticity in Higher Dimensions

In this section, we consider hyperelasticity models for two and three dimensions. A hyperelastic material is a material for which a type of constitutive model exists, for which the stress-strain relationship is derived from a strain energy density function. Given a solid body $\Omega \subset \mathbb{R}^n$ we define the displacement field as $u : \Omega \to \mathbb{R}^n$. This transforms the undeformed body $\Omega$ to a deformed body $\tilde{\Omega} = u(\Omega) \subset \mathbb{R}^n$.

## 4.1 Deformation of a Hyperelastic Beam (2D)

Here, we follow the example shown in [FBB16, Sec. 4.4]. Recall that in Section 3 we modelled the deformation of a beam under compression with Euler's elastica equation (3.2). In this subsection, we model an analogue of this. In particular, we model the two-dimensional compressible neo-Hookean hyperelastic PDE, solved again in the computational platform FEniCS. Hyperelastic models are characterized by the existence of a stored strain energy density function $\psi$.

The potential energy $\Pi$ is given by

$$\Pi(u) = \int_\Omega \psi(u)\,\mathrm{d}x - \int_\Omega B \cdot u\,\mathrm{d}x - \int_{\partial\Omega} T \cdot u\,\mathrm{d}s, \tag{4.1}$$

where $\Omega$ represents the domain, $u : \Omega \to \mathbb{R}^2$ represents the displacement, $\psi$ is the stored strain energy density, $B$ is the body force per unit area, and $T$ is the traction force per unit length. Let us first consider the deformation gradient

$$F = I + \nabla u, \tag{4.2}$$

the right Cauchy-Green tensor

$$C = F^\top F, \tag{4.3}$$

the isochoric decomposition of $C$ given by $J = \det(F)$ and the principal invariant $I_c = \mathrm{tr}(C)$. The compressible neo-Hookean stored energy density is given by

$$\psi = \frac{\mu}{2}(I_c - 2) - \mu \log(J) + \frac{\lambda}{2}\log(J)^2, \tag{4.4}$$

where $\mu$ and $\lambda$ are the Lamé parameters, which are calculated from the Young's modulus $E$ and the Poisson ratio $\nu$, as

$$\lambda = \frac{E\nu}{(1+\nu)(1-2\nu)} \quad \text{and} \quad \mu = \frac{E}{2(1+\nu)}. \tag{4.5}$$

For this problem, we choose $\Omega = (0,1) \times (0,0.1)$ which in FEniCS is translated as

```
mesh = RectangleMesh(Point(0,0),Point(1,0.1),64,64)
```

where we discretise the equation with 64 linear finite elements in the horizontal direction and also 64 in the vertical direction, using FEniCS and PETSc. Notice that since we are working in 2D now, we need to define $V$ as a vector function space

```
V = VectorFunctionSpace(mesh, "Lagrange", 1)
```

We again choose to terminate Newton's method if convergence is not achieved within the first 100 iterations.

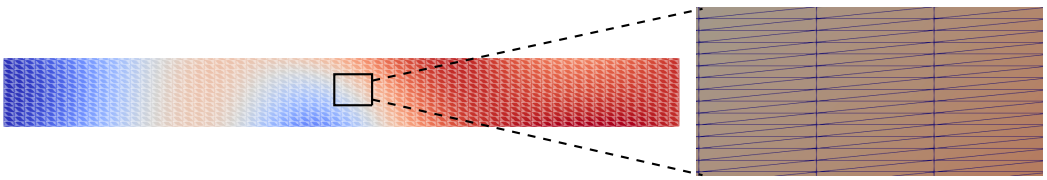

Figure 4.1: Zoomed in section of the finite element discretisation.

In this report as in [FBB16, Sec. 4.4], we choose the following parameters: gravitational body force $B = (0, -1000)$, traction $T = 0$, $E = 10^6$ and $\nu = 0.3$. Furthermore, we impose Dirichlet boundary conditions on the left and right boundaries

$$u(0,\cdot) = (0,0), \qquad u(1,\cdot) = (-\varepsilon, 0), \tag{4.6}$$

where $\varepsilon$ is the parameter to be numerically continued.

```
xl = CompiledSubDomain("(std::abs(x[0]) < DOLFIN_EPS) && on_boundary")
xr = CompiledSubDomain("(std::abs(x[0]-1) < DOLFIN_EPS) && on_boundary")
```

```
# Specify the constant eps
eps = Constant(0.2)

# Define Dirichlet boundary (x = 0 or x = 1)
bcl = DirichletBC(V, (0.0, 0.0), xl)
bcr = DirichletBC(V, (-eps, 0.0), xr)
bcs = [bcl, bcr]
```

We wish to compute minimizers of (4.1) by seeking solutions $u \in V_\varepsilon$ such that

$$\Pi'(u; v) = 0 \text{ for all } v \in V, \tag{4.7}$$

where for a fixed $\varepsilon$ we have $V_\varepsilon = \{u \in H^1(\Omega; \mathbb{R}^2) : u(0, \cdot) = (0, 0), u(1, \cdot) = (-\varepsilon, 0)\}$. At minimum points of $\Pi$, the Gâteaux derivative of $\Pi$ is zero for all displacement fields, i.e.

$$\left.\frac{\mathrm{d}\Pi(u + \tau v)}{\mathrm{d}\tau}\right|_{\tau=0} = 0 \qquad \text{for all } v \in V. \tag{4.8}$$

```
# Strain energy density for compressible neo-Hookean model
psi = (mu/2)*(Ic - 2) - mu*ln(J) + (lambd/2)*(ln(J))**2

# Potential energy
Pi = psi*dx - dot(B, u)*dx - dot(T, u)*ds

# Compute Gateaux derivative of Pi
F = derivative(Pi, u, v)
```

Since the problem is nonlinear, we must find the Jacobian of (4.8) to solve the problem using Newton's method.

We solve (4.7) from $\varepsilon = 0$ to $\varepsilon = 0.2$, with small continuation steps of the form

```
for eps_val in list(np.linspace(0.1275, 0.2, 500)):
```

Note that using different initial values in the numerical continuation process, we can essentially recover different solutions to (4.7). The 'trick' is to take very small steps between the disconnected parts of the bifurcation diagram to switch between different solution branches. Some of the solutions are shown in Figure 4.2.

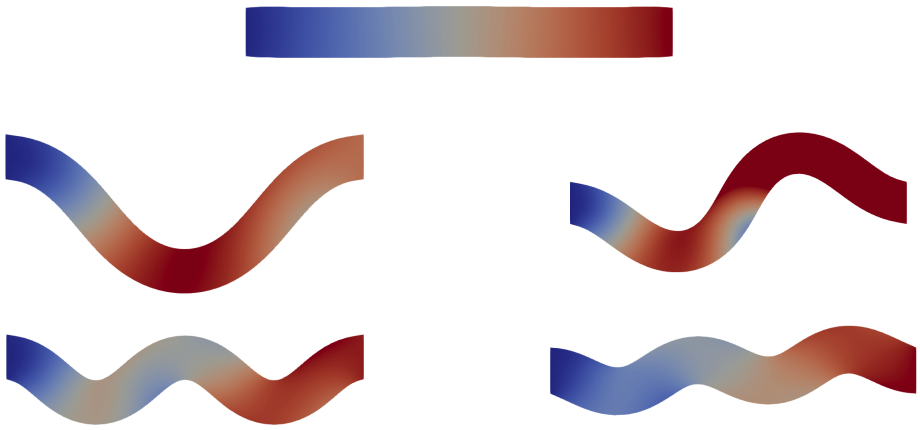

Figure 4.2: A sample of the solutions of the hyperelastic PDE (4.7) for $\varepsilon = 0.2$. The color refers to the magnitude of the displacement of the reference configuration, with blue being smaller than red. All subfigures are plotted with different color bars.

Note that solutions of the opposite sign also exist. For example, for the first buckling eigenmode the following shape was found in [FBB16, Fig. 4.5]

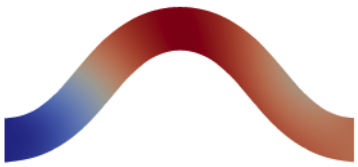

The authors of [FBB16] used a powerful algorithm for computing bifurcation diagrams, called *deflated continuation*, however, the algorithm is not implemented in this report. The bifurcation diagram would be symmetric about the $\varepsilon$-axis[1] if we chose both applied forces to be zero, i.e. $B = 0$ and $T = 0$. As the parameter $\varepsilon$ is increased, the diagram undergoes a series of bifurcations, but since we are imposing a gravitational body force $B$, the reflective symmetry is broken and the bifurcation diagram is disconnected.

## 4.2 Deformation of a Hyperelastic Cuboid (3D)

In this report, we present a hyperelastic model to study the effect of twisting a cuboid made up of a hyperelastic material. This is inspired by the demo example in hyperelasticity, as described in [LMW12]. More specifically, we investigate the behaviour of

[1] This is also known as a $\mathbb{Z}_2$ reflective symmetry. In general, the $\mathbb{Z}_n$ group describes a symmetry of a plane figure invariant after a rotation of $2\pi/n$ degrees.

the three-dimensional compressible Mooney-Rivlin model and show briefly the results of using the neo-Hookean model in Appendix C.

In Table 2, we present the material parameters used in the numerical implementation of the two hyperelasticity models.

| Description | Value |
|---|---|
| $E$, Young's modulus | $10^6$ |
| $\nu$, Poisson ratio | 0.3 |
| $\kappa$, bulk modulus | $\frac{E}{3(1-2\nu)}$ |
| $\mu$, Lamé parameter | $\frac{E}{2(1+\nu)}$ |
| $\lambda$, Lamé parameter | $\frac{E\nu}{(1+\nu)(1-2\nu)}$ |

Table 2: Material parameter specification for three-dimensional cuboid models.

For both hyperelasticity models in this report, we use: gravitational body force $B = (0.0, -0.5, 0.0)$ and traction force on the boundary $T = (1.0, 0.0, 0.0)$. Furthermore, the boundary conditions that ensure a twisting by 60° are given by Dirichlet boundary conditions on $\Gamma_0 = 0 \times (0,1) \times (0,1)$ and $\Gamma_1 = 1.25 \times (0,1) \times (0,1)$

$$u|_{\Gamma_0} = \begin{pmatrix} 0 \\ 0 \\ 0 \end{pmatrix} \text{ and } u|_{\Gamma_1} = \begin{pmatrix} 0 \\ 0.5[0.5 + (y-0.5)\cos(\pi/3) - (z-0.5)\sin(\pi/3) - y] \\ 0.5[0.5 + (y-0.5)\sin(\pi/3) + (z-0.5)\cos(\pi/3) - z] \end{pmatrix},$$

where $u$ is the displacement field. The cuboid has dimensions $(0, 1.25) \times (0,1) \times (0,1)$.

### 4.2.1 Mooney-Rivlin 3D model

Here we study the Mooney-Rivlin hyperelastic model [Moo40, Riv48]. Let us introduce the relevant invariants of the right Cauchy-Green tensor. We have $J = \det(F)$, the principal invariants of the isochoric part $I_1 = \mathrm{tr}(C)$ and $I_2 = \frac{1}{2}\left[\mathrm{tr}(C)^2 - \mathrm{tr}(C^2)\right]$. The compressible Mooney-Rivlin stored energy density function $\psi$ is given by

$$\psi = c_1(I_1 - 3) + c_2(I_2 - 3) + \kappa(J-1)^2, \tag{4.9}$$

where $c_1$ and $c_2$ are material constants. In the implementation we arbitrarily choose $c_1 = \mu/2$ and $c_2 = \mu/4$. If we chose $c_1 = \mu/2$ and $c_2 = 0$, then we would recover the compressible neo-Hookean solid, which is a special case of a Mooney-Rivlin solid, with a stored energy density function given by (C.1), found in Appendix C.

The results are shown in Figure 4.3, with the elasticity parameters as shown in Table 2. Note that the result is the same (both qualitatively and quantitatively)

whether the compressible neo-Hookean or the Mooney-Rivlin model is used, and so the model works for different materials. See Figure C.1.

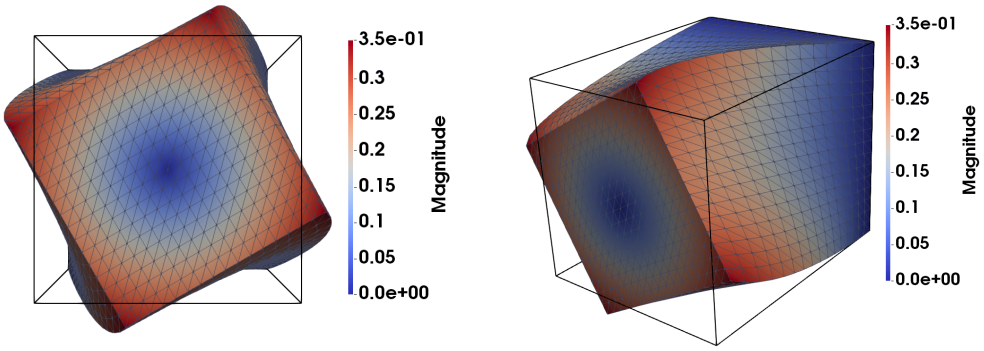


Figure 4.3: Deformation of a Mooney-Rivlin cuboid of dimensions $x = 1.25$, $y = z = 1$ after twisting it through 60°. The black outline is the initially undeformed cuboid.

# 5 Conclusion

In this report, we investigated numerically the deformation of two different cases of 1D elastic beams and determined the accuracy of our code using the method of manufactured solutions. We also studied 2D hyperelastic beams and the deformation of hyperelastic cuboids under twisting. These problems were solved using FEniCS which is a powerful tool for implementing the finite element method. We found that in some cases, applying a certain forcing load, causes the beams to exhibit interesting behaviour, such as buckling, which results in various eigenmodes.

An interesting extension to this work would be to study the deformation of bodies composed of multiple materials or the bifurcation of buckling of spherical caps under hydrostatic pressure or some load system, as illustrated in Figure 5.1. In this problem, the parameter $\lambda$ would denote the hydrostatic pressure and $u$ the measure of distortion from the uniform spherical configuration. This problem would also have an associated bifurcation diagram.

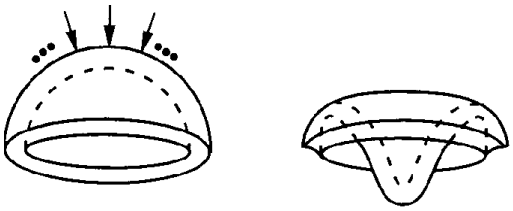

Figure 5.1: Buckling of a spherical cap under hydrostatic pressure [Ant05, Fig. 2.9].

# References


[All07] G. Allaire. *Numerical analysis and optimization: an introduction to mathematical modelling and numerical simulation.* Oxford University Press, 2007.

[Ant05] S. Antman. *Nonlinear problems of elasticity (2nd ed., Applied mathematical sciences).* New York: Springer, 2005.

[FBB16] P. E. Farrell, C. H. L. Beentjes, and Á. Birkisson. The computation of disconnected bifurcation diagrams. *arXiv preprint arXiv:1603.00809*, 2016.

[HKO09] P. Howell, G. Kozyreff, and J. Ockendon. *Applied solid mechanics*, volume 43. Cambridge University Press, 2009.

[KA68] J. B. Keller and S. S. Antman. Bifurcation theory and nonlinear eigenvalue problems, 1967. 1968.

[LMW12] A. Logg, K-A. Mardal, and G. Wells. *Automated solution of differential equations by the finite element method: The FEniCS book*, volume 84. Springer Science & Business Media, 2012.

[MH94] J. E. Marsden and Thomas J. R. Hughes. *Mathematical foundations of elasticity.* Courier Corporation, 1994.

[Moo40] M. Mooney. A theory of large elastic deformation. *Journal of applied physics*, 11(9):582–592, 1940.

[Rei69] E. L. Reiss. *Column buckling-An elementary example of bifurcation in "Bifurcation Theory and Nonlinear Eigenvalue Problems, J.B. Keller and S. Antman".* Benjamin, New York, 1969.

[Riv48] R. S. Rivlin. Large elastic deformations of isotropic materials. iv. further developments of the general theory. *Philosophical Transactions of the Royal Society of London A: Mathematical, Physical and Engineering Sciences*, 241(835):379–397, 1948.

[Roa02] P. J. Roache. Code verification by the method of manufactured solutions. *Transactions-American Society of Mechanical Engineers Journal of Fluids Engineering*, 124(1):4–10, 2002.

# Appendix A More on Diving Boards

In this appendix we present some analytical results on the problem of the deforming diving board under a forcing load. If we multiply (2.9) by $\frac{\mathrm{d}\theta}{\mathrm{d}s}$ and integrate once with respect to $s$, we obtain the following equation

$$\left(\frac{\mathrm{d}\theta}{\mathrm{d}s}\right)^2 = \frac{2F}{EI}(\sin\theta + \sin\alpha), \tag{A.1}$$

where $\alpha = -\theta(L)$. When taking the square root, we note that we expect $\frac{\mathrm{d}\theta}{\mathrm{d}s}$ to be negative and thus obtain the solution in parametric form as

$$\int_0^{-\theta} \frac{\mathrm{d}\tilde{\theta}}{\sqrt{\sin\alpha - \sin\tilde{\theta}}} = s\sqrt{\frac{2F}{EI}}, \tag{A.2}$$

where $\theta = -\alpha$ when $s = L$, and so we can write the transcendental equation

$$\int_0^{\alpha} \frac{\mathrm{d}\tilde{\theta}}{\sqrt{\sin\alpha - \sin\tilde{\theta}}} = L\sqrt{\frac{2F}{EI}}, \tag{A.3}$$

which can be written in terms of so-called elliptic integrals.

# Appendix B MAPLE code for MMS

For finding the source term in the method of manufactured solutions we had to use the software MAPLE. The code is shown below for both one-dimensional elasticity problems. We start with the diving board example.

```
> # we wish to find the right hand side f for the method of manufactured solutions for
  the deflection of a diving board
> # first let us define out manufactured exact solution
> uexact := 1-cos(2*Pi*x/(1+x*(1-x)))
```

$$uexact := 1 - \cos\left(\frac{2\,\pi\,x}{1 + x\,(1 - x)}\right) \tag{1}$$

```
> # we want to verify whether our manufactured exact solution satisfies the appropriate
  boundary condtions. Thus we first differentiate once with respect to x
> firstDeriv:=diff(uexact, x)
```

$$firstDeriv := \left(\frac{2\,\pi}{1 + x\,(1 - x)} - \frac{2\,\pi\,x\,(1 - 2\,x)}{(1 + x\,(1 - x))^2}\right)\sin\left(\frac{2\,\pi\,x}{1 + x\,(1 - x)}\right) \tag{2}$$

```
> # evaluate this at x=1
> eval((2*Pi/(1+x*(1-x))-2*Pi*x*(1-2*x)/(1+x*(1-x))^2)*sin(2*Pi*x/(1+x*(1-x))), x = 1)
```

$$0 \tag{3}$$

```
> # now let us substitute this into Euler elastica equation
> diff(uexact, x, x)+FEI*cos(uexact)
```

$$\left(-\frac{4\,\pi\,(1 - 2\,x)}{(1 + x\,(1 - x))^2} + \frac{4\,\pi\,x\,(1 - 2\,x)^2}{(1 + x\,(1 - x))^3} + \frac{4\,\pi\,x}{(1 + x\,(1 - x))^2}\right)\sin\left(\frac{2\,\pi\,x}{1 + x\,(1 - x)}\right) + \left(\frac{2\,\pi}{1 + x\,(1 - x)} - \frac{2\,\pi\,x\,(1 - 2\,x)}{(1 + x\,(1 - x))^2}\right)^2\cos\left(\frac{2\,\pi\,x}{1 + x\,(1 - x)}\right) + FEI\cos\left(-1 + \cos\left(\frac{2\,\pi\,x}{1 + x\,(1 - x)}\right)\right) \tag{4}$$

```
> # the simplified version of this will be our source function f
> f:=simplify(%)
```

$$f := \frac{1}{(x^2 - x - 1)^4}\left(FEI\,(x^2 - x - 1)^4\cos\left(-1 + \cos\left(\frac{2\,\pi\,x}{x^2 - x - 1}\right)\right) + 4\left(\left(x^2 - x - 1\right)\left(x^3 + 3\,x - 1\right)\sin\left(\frac{2\,\pi\,x}{x^2 - x - 1}\right) + \pi\cos\left(\frac{2\,\pi\,x}{x^2 - x - 1}\right)\left(x^2 + 1\right)^2\right)\pi\right) \tag{5}$$

The following MAPLE code is used to determine $f$ for the Euler's elastica problem.

```
> # we wish to find the right hand side f for the method of manufactured solutions for
  Euler's elastica problem
> # first let us define out manufactured exact solution
> uexact := 1-cos(2*Pi*x/(1+x*(1-x)))
```

$$uexact := 1 - \cos\left(\frac{2\,\pi\,x}{1 + x\,(1 - x)}\right) \tag{1}$$

```
> # now let us substitute this into Euler elastica equation
> diff(uexact, x, x)+lambda^2*sin(uexact)
```

$$\left(-\frac{4\,\pi\,(1 - 2\,x)}{(1 + x\,(1 - x))^2} + \frac{4\,\pi\,x\,(1 - 2\,x)^2}{(1 + x\,(1 - x))^3} + \frac{4\,\pi\,x}{(1 + x\,(1 - x))^2}\right)\sin\left(\frac{2\,\pi\,x}{1 + x\,(1 - x)}\right) + \left(\frac{2\,\pi}{1 + x\,(1 - x)} - \frac{2\,\pi\,x\,(1 - 2\,x)}{(1 + x\,(1 - x))^2}\right)^2\cos\left(\frac{2\,\pi\,x}{1 + x\,(1 - x)}\right) - \lambda^2\sin\left(-1 + \cos\left(\frac{2\,\pi\,x}{1 + x\,(1 - x)}\right)\right) \tag{2}$$

```
> # the simplified version of this will be our source function f
> f:=simplify(%)
```

$$f := \frac{1}{(x^2 - x - 1)^4}\left(-\lambda^2\left(x^2 - x - 1\right)^4\sin\left(-1 + \cos\left(\frac{2\,\pi\,x}{x^2 - x - 1}\right)\right) + 4\left(\left(x^2 - x - 1\right)\left(x^3 + 3\,x - 1\right)\sin\left(\frac{2\,\pi\,x}{x^2 - x - 1}\right) + \pi\cos\left(\frac{2\,\pi\,x}{x^2 - x - 1}\right)\left(x^2 + 1\right)^2\right)\pi\right) \tag{3}$$

# Appendix C Nonlinear Elasticity Summary

In Subsection 4.2, we started with a theoretical background leading to the necessary governing equations. We attained a weak form that was used in the code to solve an example on a simple geometry, a cuboid. The weak form is valid for any geometry, so the code can be used in other cases.

| Description | Formula |
|---|---|
| Infinitesimal strain tensor | $\epsilon = \frac{1}{2}\left(\nabla u + \nabla u^\top\right)$ |
| Deformation Gradient | $F = 1 + \nabla u$ |
| Right Cauchy-Green tensor | $C = F^\top F$ |
| Green-Lagrange strain tensor | $E = \frac{1}{2}(C - 1)$ |
| Volumetric and isochoric decomposition of $C$ | $\overline{C} = J^{-2/3}C$, $J = \det(F)$ |
| Principal invariants of $C$ | $I_1 = \mathrm{tr}(C)$, $I_2 = \frac{1}{2}[\mathrm{tr}(C)^2 - \mathrm{tr}(C^2)]$, $I_3 = \det(C)$ |

Table 3: Definitions of some common strain measures [LMW12, pp. 528].

The material model is general enough to allow for us to consider different popular material models such as

1. St. Venant-Kirchhoff model: $\psi = \frac{\lambda}{2}\mathrm{tr}(E)^2 + \mu\mathrm{tr}(E^2)$,
2. Mooney-Rivlin model: $\psi = c_1(I_1 - 3) + c_2(I_2 - 3) + \kappa(J-1)^2$.

## C.1 Neo-Hookean 3D model

We also considered a three-dimensional compressible neo-Hookean hyperelastic PDE, that that we solved in FEniCS. The same constitutive equations as in Section 4.1 hold. Given that now we are working in a three-dimensional frame, the compressible neo-Hookean stored energy density is now given by

$$\psi = \frac{\mu}{2}(I_c - 3) - \mu\log(J) + \frac{\lambda}{2}\log(J)^2. \tag{C.1}$$

Note the difference in the $\log(J)^2$ and $(J-1)^2$ terms. The precise form of this term is not important as long as it reduces to zero when $J$ is approximately 1 and it quickly increases when $J$ deviates from 1.

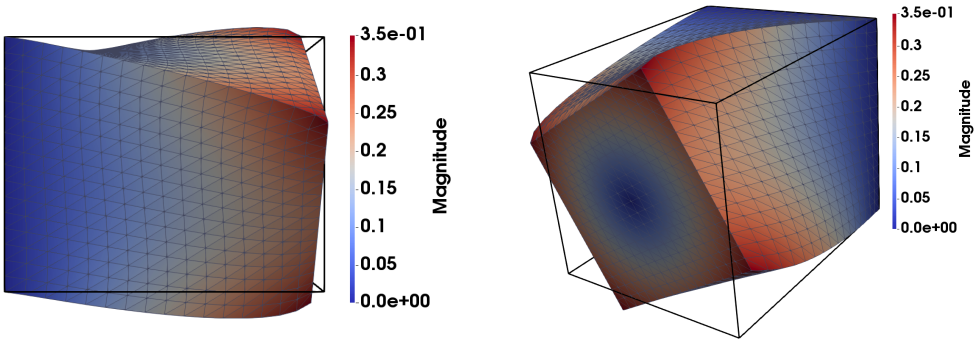


Figure C.1: Deformation of a neo-Hookean cuboid of dimensions $x = 1.25$, $y = z = 1$ after twisting it through 60°. The black outline is the initially undeformed cuboid.